



International Atomic Energy Agency

INDC(GDR)-18/L

---

**INDC**

**INTERNATIONAL NUCLEAR DATA COMMITTEE**

---

PEAK SEPARATION FROM TIME-OF-FLIGHT SPECTRA  
AND PROBLEMS OF DETECTOR EFFICIENCY DETERMINATION  
IN NEUTRON SPECTROSCOPY

D. Schmidt and D. Seeliger  
Technical University Dresden, GDR

September 1982

---

**IAEA NUCLEAR DATA SECTION, WAGRAMERSTRASSE 5, A-1400 VIENNA**

Reproduced by the IAEA in Austria  
September 1982

PEAK SEPARATION FROM TIME-OF-FLIGHT SPECTRA  
AND PROBLEMS OF DETECTOR EFFICIENCY DETERMINATION  
IN NEUTRON SPECTROSCOPY

D. Schmidt and D. Seeliger  
Technical University Dresden, GDR

September 1982

## Table of Contents

	Page
Abstract	
1. Introduction	1
2. Mathematical representation of neutron lines	2
3. Properties of the analytical function used	4
4. Peak separation from neutron spectra	6
5. Efficiency determination methods	11
6. Problems related to the use of the $^{252}\text{Cf}$ method	13
References	16
Tables, Figures	

## Abstract

An analytical expression for real neutron line representation is discussed in detail. In connection with elastic peaks from a small carbon sample this function can give a convenient model line to separate elastic peaks from continuous spectra. This problem is also discussed.

Using the  $^{252}\text{Cf}$  method for efficiency determination the experimental points have to be continue to higher energies. Related problems are discussed and illustrated by examples.

Peak separation from TOF-spectra and problems of detector efficiency determination in neutron spectroscopy

D.Schmidt and D.Seeliger

Technical University Dresden, GDR

1. Introduction

Peak separation from neutron TOF-spectra and determination of neutron detector efficiency are important and general problems in the field of fast neutron spectroscopy. Both problems show the direct connection between development of experimental technique and also data routing with computer codes.

Peak separation of isolated lines is generally a simple problem. But for unfolding of overlapping lines or separation of peaks from continuous spectra some methodical experience is necessary. The results of the represented paper show that especially the high energy part of continuous inelastic neutron spectra depends as well in shape as magnitude on the separation method of elastic neutron peak.

An other general problem is the efficiency curve determination for the neutron detectors. This point influences mostly on the magnitude of uncertainty which can be obtained in neutron scattering experiments. In order to determine the efficiency curve several methods have been developed. But most of them need an accelerator based source of monoenergetic neutrons. Recently the 252-Cf method was introduced. In this way it is possible to measure exactly the efficiency curve in the MeV-region. For higher energies a completion by calculation or other methods is necessary. This paper gives experience also in this field.

The results represented here have been obtained using a multi-angle neutron TOF-spectrometer consisting of eight detectors /1/ with their individual properties which have been checked in this way. However, these results seem to be useful also for experiments with one detector or under other conditions.

## 2. Mathematical representation of neutron lines

In the most cases, neutron lines within a TOF-spectrum are unsymmetric to larger flight time, that means to lower energy. Fig.1 shows neutron lines from a deuterium gas target /2/ in order to demonstrate deviations from symmetric Gaussian shape. The shape of neutron lines is influenced mainly by the following circumstances:

- (1) The energy spectrum within the neutron pulse is asymmetric to lower energies due to the non-linear stopping power of charged particles and by multiple scattering on the nuclei within the target, the scattering sample and shielding material, respectively.
- (2) Normally, the trigger moment of the time signal depends on the corresponding proton recoil energy. Therefore, an asymmetric portion of the neutron peak is obtained. This effect can be reduced by electronic equipment or by means of a computer.
- (3) The flight time throughout the scintillator gives an additional time spread. For thin scintillators where the expression  $1 - \exp(-n\sigma d_{\text{scint}})$  can be approximated by  $n\sigma d_{\text{scint}}$  this time spread is symmetric around the geometric centre of the scintillator. Therefore, this effect gives a symmetric component to the asymmetric neutron pulse, which increases with lower neutron energy ( $\Delta t_{\text{scint}}$  is proportional to  $d_{\text{scint}} \cdot (E_n)^{-1/2}$ ). Only for thick scintillators this time spread will be asymmetric because the detection probability depends on the neutron path inside the scintillator.
- (4) The concrete operation mode of the pulsing electronics shows a remarkable influence on the pulse shape because of the energy dependence of accelerator transmission. The time structure of the ion pulse is caused mainly by energy modulation, so the beam loss in the different ionoptic elements is accomplished by change of time structure, i.e. pulse shape. The pulsing electronics is adjusted by eye-controlled TOF-spectrum to realize a minimum asymmetry and fwhm, respectively. Despite that the line shape in the spectra is expected to be different not

only for different incident energies, but also in different measuring periods at the same incident energy. For peak unfolding individual detector properties have to be taken into consideration by choice of a proper analytical representation, especially using a number of detectors as in multi-angle detector systems. Therefore, the following mathematical expressions are included into the investigation (see also figs. 1 and 2):

(a) symmetrical Gaussian curve:

$$f(x) = N \frac{0.565}{\sqrt{2} \sigma} \exp(-|(x-x_0)/\sqrt{2} \sigma|^\beta) \quad (2.1)$$

In the normal case this expression cannot be used. (The exponent  $\beta$  can deviate from the well known, typical value  $\beta = 2$ .)

(b) double-symmetrical Gaussian curve:

$$f(x) = \begin{cases} N \frac{0.565}{\sqrt{2} \sigma_1} \exp(-|(x-x_0)/\sqrt{2} \sigma_1|^\beta) \\ N \frac{0.565}{\sqrt{2} \sigma_2} \exp(-|(x-x_0)/\sqrt{2} \sigma_2|^\beta) \end{cases} \quad \text{for } x \geq x_0 \quad (2.2)$$

with  $\sigma_2 > \sigma_1$ .

(c) Gaussian curve with exponential continuation at the left side:

$$f(x) = \begin{cases} N \exp(-(x-x_0)^2/2 \sigma^2) \\ N \exp((b^2+2bx-2bx_0)/2 \sigma^2) \end{cases} \quad \text{for } x \geq (x_0-b) \quad (2.3)$$

This function could be an adequate expression to describe neutron lines. But the peak area cannot be derivated from this expression analytically.

(d) folding of an exponential function with a Heaviside distribution /3/:

$$f(x) = N(\lambda N_1)^{-1} \exp((x-x_0)/\lambda + \sigma^2/2\lambda^2) \quad (2.4)$$

with the denominator  $N_1$

$$N_1 = 1 + \exp \left[ 2.25178 \left( \frac{x-x_0}{\sqrt{2}\sigma} + \frac{\sigma}{\sqrt{2}\lambda} \right) + 0.202197 \left( \frac{x-x_0}{\sqrt{2}\sigma} + \frac{\sigma}{\sqrt{2}\lambda} \right)^3 \right]$$

This expression is used in the paper represented here and realized in the code ASYVAR-1 /4/. It will be discussed in detail below.

(e) superposition of a curve according to (d) with a symmetric Gaussian function (a):

$$f(x) = f(x)_{(d)} + Af(x)_{(a)}$$

This function type has been developed to describe  $\gamma$ -lines /5/, but it is also not appropriate for our purpose, see fig.1.

From these possibilities (a) ... (e) the function (d) has been selected because it is realized in computer code and has been used to unfold line spectra from (p,n) reactions successfully. This function is discussed in detail in the following.

### 3. Properties of the analytical function used

(i) analytical expression:

$$f(x;N,x_0,\sigma,\lambda) = \frac{N}{\sigma} \exp\left(\sqrt{2}\frac{\sigma}{\lambda}y - \frac{1}{2}\left(\frac{\sigma}{\lambda}\right)^2\right) \frac{\sigma/\lambda}{1+\exp(2.252y + 0.2022y^3)}$$

$$\text{with } y = (x-x_0)/\sqrt{2}\sigma + \sigma/\sqrt{2}\lambda \quad (2.5)$$

The parameter N represents the full peak area; the parameters  $x_0$ ,  $\sigma$  and  $\lambda$  correspond to the position, fwhm and asymmetry, respectively, but they are not identical with them.

(ii) position of the peak maximum  $x_m$ :

The condition  $d/dxf(x;N,x_0,\sigma,\lambda) = 0$  gives an implicit expression

$$\sigma/\lambda = g(y_m) \quad \text{with} \quad y_m = (x_m-x_0)/\sqrt{2}\sigma + \sigma/\sqrt{2}\lambda$$

$$\text{and} \quad x_m = x_0 - \sqrt{2}\sigma(\sigma/\sqrt{2}\lambda - y_m) \quad (2.6)$$

For given  $y_m$  one can calculate the corresponding ratio  $\sigma/\lambda$

and therefore replace

$$x_m = x_0 - a \cdot \sigma, \quad a = f_1\left(\frac{\sigma}{\lambda}\right) \quad (2.7)$$

whereby the parameter  $a$  can be given numerically for values  $\sigma/\lambda$  (see table 1).

(iii) centre of mass of the peak area  $x_{cm}$ :

The centre of mass  $x_{cm}$  can be calculated explicitly if the function  $f(x; N, x_0, \sigma, \lambda)$  is normalized

$$\int_{-\infty}^{+\infty} f(x; N, x_0, \sigma, \lambda) dx = N \quad (2.8)$$

From  $x_{cm} = \frac{1}{N} \int x f(x; N, x_0, \sigma, \lambda) dx$  follows

with  $\eta = \sqrt{2} \sigma / \lambda$

$$\int \frac{e^{\eta y} dy}{1 + \exp(2.25y + 0.202y^3)} = \frac{1}{\eta} e^{\eta^2/4} \quad (2.9)$$

and

$$\int y \frac{e^{\eta y} dy}{1 + \exp(2.25y + 0.202y^3)} = \frac{\partial}{\partial \eta} \left( \frac{1}{\eta} e^{\eta^2/4} \right) \quad (2.10)$$

the result

$$x_{cm} = x_0 - \lambda \quad (2.11)$$

If one requires an asymmetry  $f(x_m - x) > f(x_m + x)$  than follows from  $x_{cm} < x_m$ :  $\lambda/\sigma > a$  and from table 1  $\sigma/\lambda < 2.41$ . The quantity  $\lambda$  characterizes the asymmetry relatively to  $\sigma$ : the smaller  $\sigma/\lambda$  the more asymmetric is the line shape (see fig.3). If  $\sigma/\lambda$  increases too much the normalization is violated and the peak area is smaller than  $N$ .

(iv) fwhm of the line:

The calculation of the fwhm is not possible analytically.

Firstly it should be taken the parabola approximation

$$f(y) \approx f(y_m) + 1/2(y - y_m)^2 d^2/dy^2 f(y_m) :$$

$$fwhm = 2\sqrt{2} \sqrt{-f(y_m)/f''(y_m)} = 2\sigma b_1 \quad (2.12)$$

whereby  $b_1$  is a function of  $\sigma/\lambda$  (see table 1):

$$b_1 = \sqrt{\frac{2z}{[\sqrt{2}\sigma/\lambda](z^2 - \sqrt{2}z\sigma/\lambda) + \sqrt{2}(\sigma/\lambda) \cdot 1.212y_m}}$$

$$z = 2.25 + 0.606y_m^2 \quad (2.13)$$

Using this method for a Gaussian function the fwhm is too small by a factor 1.18. This factor is added empirically to eq. (2.13), and so a very good agreement of this expression

$$\text{fwhm} = 2.36\sigma b_1 = 2\sigma b, \quad b = 1.18b_1 = f_2(\sigma/\lambda) \quad (2.14)$$

with real line shapes is obtained. That is demonstrated in fig.4.

Table 1 gives numerical values for the quantities a and b outgoing from the auxilliary quantity  $y_m$ .

The expression  $\sigma f(x_m)/N$  should increase with  $\sigma/\lambda$  (a more symmetric line has a higher maximum); that is the case up to  $\sigma/\lambda < 2.36$ . Furthermore, the following values  $\sigma f(x_m)/N > 1$  are without sense. In the computer code ASYVAR-1 a maximum value  $\sigma/\lambda = 2.40$  is admissible. For higher values needed to reach the  $\chi^2$ -minimum the code turns to functions of Gaussian type.

Using this function, real lines have been calculated where x and f(x) were integers. The properties (fwhm, centre of mass, normalization) of these lines are drawn and compared with the analytical expressions in fig.4.

#### 4. Peak separation from neutron spectra

First question is to find out general properties of the code ASYVAR-1 using model lines constructed. Firstly two model lines with different peak area ratio and distance, respectively, have been unfolded by this code. The result is given in table 2. There is demonstrated that line separation for distances smaller than  $0.5\text{fwhm}$  doesn't seem to be useful.

In order to study the line separation from linear background (see fig.5), it has been investigated the influence of separation mode and line shape parameters, respectively. The results obtained are listed in table 3.

Because the straight line background corresponds to the spectrum construction, this shape of background gives naturally the best fit results for all operation ranges (the small  $\chi^2/F$  ratio is understandable because of construction of the spectrum; the computer code takes as error than simply  $\sqrt{N}$ ). The second mode with constant background corresponds to a fit only on the right side of line. Thereby the background below the peak is taken as peak area, and in this way the peak area is overestimated. If than  $\sigma$  and  $\lambda$  were changed, the error becomes higher due to the absence of any information about the asymmetry (left side) of the line.

The next question is to look for model lines which are adequate and available:

- The  $\gamma$ -lines from the TOF-spectrum cannot be taken because its line shape is quite different from that of neutron lines.
- The direct line from the neutron target can be used if the influence of the sample (time spread due to geometry, multiple scattering) is considered via Monte Carlo calculation. This way is demonstrated in ref. /6/ .
- Experimental peaks from elastic scattering on nuclei with relatively high-lying first excited state (12-C, 40-Ca, 208-Pb et al.) can be used to extract model line parameters. In this case, additionally one has to investigate the influence of multiple scattering on line shape depending on mass number. This effect should be dependent also on sample size. Table 4 shows that for two quite different samples of carbon the asymmetry averaged over all detectors and expressed by  $\lambda/\sigma$  is independent from sample size. This fact can be understood also in connection with fig.6. There is given a real elastic peak from the 12-C(n,n) reaction and the fit with the analytical function  $f(x;N,x_0,\sigma,\lambda)$ . The multiple scattering tail at the low-energy side doesn't influence the fit procedure because of its order of some percent.

Table 5 gives the averaged (over all detectors, in order to see general tendencies) fwhm and asymmetry  $\lambda/\sigma$  for the  $n_0$ - and  $n_1$ -group of  $^{12}\text{C}(n,n')$  reaction at two different energies. These results confirm the general remarks above concerning properties of neutron TOF-lines.

The conclusion is that the use of small carbon sample gives quite good neutron model lines in connection with the analytical expression applied. This method seems to be equivalent to modify direct neutron peaks with Monte Carlo calculations.

For separation of lines from TOF-spectra one has to distinguish the following cases.

- (A) Unfolding of a "pure" line spectrum to get partial cross sections

In this case the remaining background (in shape and magnitude) is not of interest. Problems occur only in connection with overlapping peaks if the line distance is too small or the peak area ratio is high. As noted above a peak separation at distances smaller than  $0.5\text{fwhm}$  is not worth while (see, for instance, fig.7:  $n_2/n_3$ -group,  $\Delta K \approx 2$  channels). If the peak area ratio is high (see fig.8) the fit has to reproduce the line distance required by kinematics and geometry. Otherwise the fit has to be repeated under changed conditions.

- (B) Separation of "disturbing" neutron lines from continuous spectra

Origin, energy and intensity of "disturbing" neutron lines are investigated in detail in ref. /2/. Their energy is smaller than the energy  $E_0$  of the DD-neutrons. Supposition for separation is the exact identification of the position of the corresponding peaks in the scattering spectra. This is possible only if the ratio

$$d\sigma_{el}/d\Omega(E_0^{\text{dist}}, \theta) / \Delta E(E_{n'}) : d^2\sigma/d\Omega dE(E_0; E_{n'}, \theta)$$

for  $E_0^{\text{dist}} = E_{n'}$  is high enough where  $\Delta E(E_{n'})$  represents the energy resolution. Using a computer code, the positions of the scattering peaks following from the  $^{12}\text{C}(n,n_0)$ ,

12-C( $n, n_1$ ), 16-O( $n, n_0$ ) and 16-O( $n, n_1$ ) reactions can be calculated for all angles including kinematic effects. The remaining background shape needed for the separation fit procedure can be chosen as constant, straight line and parabolic curve, respectively, depending on the part of spectrum (see fig.9). An example for separation can be seen in fig.10. For such procedure it has to be proofed that the remaining background, i.e. the continuous spectrum, shows a smooth behaviour without significant structure (peaks or valleys). This separation method is felt to remove the natural structure of the spectrum which can follow from fluctuations and unresolved residual nucleus states, respectively. An other possibility to separate such disturbing lines is the calculation of this scattering effect from the incident  $O^0$ -spectrum. This idea has been realized in the code NEUKOR which is published elsewhere /7/ .

- (C) The separation of elastic peaks from continuous spectra can be made in a most simple mode by free fit procedure. This method is not sufficiently exact especially at forward angles: The background spectrum can be strongly time-correlated (so called "direct background peak" from the target by insufficient shielding) and furthermore the inelastic scattering effect is in order of some percents with respect to the elastic peak. In this way a free separation can give under the elastic peak negative continuum or other unphysical effects. That requires the use of model lines in spite of spending more measuring time.

The shape of model lines (parameters  $\sigma$  and  $\lambda$ ) are taken from the elastic carbon peaks discussed above. The fit procedure has to find peak area  $N$  and position  $x_0$  with consideration of a proper background shape, whereby a parabolic curve doesn't seem to be sufficiently convenient, see fig.9. Therefore, the following separation modes have been investigated and compared:

- (m1) -  $\sigma$  and  $\lambda$  from 12-C( $n, n$ ), background = straight line, spectrum part from point 2 to 5;

(m2) -  $\sigma$  and  $\lambda$  from 12-C(n,n), background = constant, spectrum part from point 4 to 6;

(m3) -  $\sigma$  and  $\lambda$  from free fit, background = straight line, spectrum part from point 2 to 5 and from point 1 to 5, respectively.

(the spectrum part for fit procedure can be taken analogously from fig.5)

In this way the following general tendencies could be obtained:

- peak area: The differences at (m2) and (m3) are small, using (m1) the peak area is smaller in order of 10...20%.
- fwhm: In the case of (m1) and (m2) the fwhm is equal per supposition, but the mode (m3) provides smaller values (4...7%).
- asymmetry: The asymmetry characterized by  $\lambda/\sigma$  increases at (m3) relatively to (m1) and (m2), for instance at  $E_0 = 7$  MeV averaged from 1.27 to 2.08.
- centre of mass: In the case of (m1)  $x_{cm}$  is shifted slightly to the right side ( $\sim 0.1$  channels corresponding 0.1 ns), but for (m3)  $x_{cm}$  is shifted to the left side relatively to (m2) ( $\sim 0.5$  channels) caused mainly by the higher asymmetry.
- remaining background: Relatively to (m2), the sum of the spectrum after elastic peak separation is higher at (m1) ( $\sim 30\%$ ) and smaller at (m3) ( $\sim 35\%$ ).

This results are demonstrated partly in fig.11.

Following from that, separation mode (m1) gives the best method in the physical sense. But it is possible only if model line parameters are determined experimentally and the elastic peak is continued smoothly to the continuous spectrum. If it is not the case (light nuclei, low bombarding energy, high energy resolution) the mode (m2)

has to be used. Using method (m3) the double-differential cross sections are too small systematically up to excitation energies  $U \lesssim 3$  MeV depending on actual time spread. Nevertheless, the time resolution of the experiment is required to be as small as possible to limit the uncertainties according to elastic peak separation.

Fig.12 shows the different separation modes in comparison using angle-integrated energy spectra of the  $93\text{-Nb}(n,n')$  reaction. The importance of this considerations for an adequate physical interpretation of the high energy tail of neutron spectra is evident.

#### 5. Efficiency determination methods

Exact determination of the detection efficiency of neutron detectors is important to reduce drastically the uncertainties of fast neutron cross sections. At present time different methods have been used and are reviewed briefly in the following. Time-of-flight technique is used mostly.

- LASL Los Alamos (USA):

Using the  $D(d,n)$ ,  $T(p,n)$ ,  $H(t,n)$  and  $7\text{-Li}(p,n)$  reactions as direct source ones a quasi-absolute measurement of efficiency curves can be realized /9/. The averaged error of this method is given to 3%. This method requires a tandem accelerator and measurement under different angles.

- AAEC Lucas Heights (Australia):

Based on associated particle method the efficiency curve can be measured absolutely /10/. This method requires a  $\Delta E$ -E-telescope for particle identification, the error is estimated to 2%.

- ANL Argonne (USA):

Based on neutron elastic scattering data from H and  $^{12}\text{C}$  as a standard the efficiency is measured absolutely using this elements /11/. Especially to provide a multi-angle detector system carbon is preferred. Recently, the  $^{252}\text{Cf}$  method additionally is introduced /12/. The error

in this way is given in order of 3...5%.

- CE Bruyères-le-Châtel (France):

In order to determine the efficiency curves (4 detector system) the relative measurement using the D(d,n) reaction directly and the absolute hydrogen scattering method are combined (see, for instance /13/). The estimated error should be 1...2%.

- FEI Obninsk (USSR):

The experimental efficiency curve is extracted relatively by use of the T(p,n) source reaction and combined with the absolute 252-Cf method /14/. The error estimated is in order of 2...5%.

- TUNL Durham (USA):

Using the D(d,n) reaction a relative efficiency curve is measured /15/. The error is given to 2.5% /16/.

- IRK Vienna (Austria):

For absolute efficiency determination two methods are combined /17/: the elastic hydrogen scattering is used as well as the 252-Cf method /18/. The error is estimated to be in order of 2%.

- TU Dresden (GDR):

The efficiency curves (8 detector system) are measured absolutely using the 252-Cf method /19/. Additionally, a check is obtained by including of elastic scattering measurement on 12-C.

Summarizing this overview the mainly used methods are direct reaction sources, scattering on "standard nuclei" and the 252-Cf method. Additionally, they are combined with several computer codes, for instance NEUCEF /20/. Using a multi-angle detector system /1/ which covers the full angle region, only the 252-Cf method is possible for simultaneous measurement. The elastic carbon scattering must be connected with exact energy calibration because of the typical resonance structure in the MeV region. On the other hand, the 252-Cf method doesn't require an accelerator and can be used for nearly all angles simultaneously. Therefore, this method is applied in the frame of this work, and the advantages and problems connected with it are discussed in detail.

## 6. Problems related to the use of the $^{252}\text{Cf}$ method

The advantages and disadvantages connected with the use of a  $^{252}\text{Cf}$  fission chamber are the following:

- (+1) For such experimental procedure no accelerator is needed.
- (+2) Using TOF-technique a sufficient energy resolution can be obtained due to available flight path.
- (+3) The background is very small for sufficiently good  $n/\gamma$ -discrimination.
- (+4) A wide angle region can be included into measurement.
- (+5) The full efficiency curve is measured simultaneously without any monitoring problems.
- (+6) The efficiency can be measured absolutely with high accuracy  $\leq 3\%$  below an energy limit depending on source strength, flight path and measuring time being available, respectively.
- (-1) For higher energies the uncertainty will increase by means of statistical errors, background subtraction or others.
- (-2) An anisotropy cannot be avoided in principle and influences on absolute normalization (see fig.13).

We conclude, that anisotropy has to be investigated experimentally and a method should be derivated to continue efficiency curves to higher energies by Monte Carlo calculations. That means one has to adjust the correct function for light response as function of energy, the energy resolution and the real detection threshold.

In the case of a multi-angle detector system the individual properties of the different detectors have to be taken into account:

- The light output response function, mostly given as relation  $L_{\text{proton}} = f(L_{\text{electron}})$  can be taken from literature, but only for complete electronic integration. In this sense the real electronic circuitry influences on this relation.
- The energy resolution of the detector depends on the scintillator type and geometry, the multiplier used and the coupling between scintillator and multiplier. In the

case of our 8 detectors the energy resolution averaged over all detectors was at the Cesium edge  $(\Delta E/E)_{Cs} = 0.34$  (0.30...0.48) and for Cobalt  $(\Delta E/E)_{Co} = 0.26$  (0.16...0.31). Extrapolating in accordance with the known energy dependence

$$(\Delta E/E)^2 = A + B \cdot E^{-1} \quad (4.1)$$

to the threshold  $E_n = 1$  MeV (equivalent to electron energy  $E_e = 0.25$ ), the energy resolution should be in order of  $(\Delta E/E)_{0.25} = 0.46$ . This value was essentially higher than expected. Furthermore, calculations can take into consideration normally only an energy-independent resolution. And there is a correlation between energy resolution and averaged height of the efficiency curve obtained in the energy region 3 to 5 MeV: the higher  $\Delta E/E$  the smaller is the averaged efficiency. This result could be obtained only by investigation of a relatively great number of different detectors.

- The background cannot be neglected if the n/ $\gamma$ -discrimination works insufficiently. In this case a time-correlated background between  $\gamma$ -peak and neutron spectrum occurs due to  $\gamma$ -production by neutrons near the collimator entrance.
- The energy linearity can be disturbed by means of saturation effects due to potential distribution of the multiplier or electronic non-linearity and can give than a deviation in the detection threshold calibrated in electron energies.

All these aspects have to be taken into account to evaluate comparison between experimental results from several detectors and calculations. Some results are averaged over all detectors for general conclusions (see also fig.14).

As demonstrated in fig.14 the calculations deviate in principle from averaged experimental points. The difference near threshold concerning the relative curve shape decreases with increasing threshold energy, which shows that the light response function used

$$\begin{aligned} E_e &= 0.215 E_p + 0.028 E_p^2 & (E_p \leq 8 \text{ MeV}) \\ E_e &= 0.6 E_p - 1.28 \text{ MeV} & (E_p > 8 \text{ MeV}) \end{aligned} \quad (4.2)$$

is not valid. The difference in absolute height between experimental points and calculated curves seems to be due to counting loss of fission products. That is underlined by the fact that the same normalization factor is necessary for the different measurements.

Using an other light response function

$$\begin{aligned} E_e &= 0.18 E_p^{3/2} & (E_p \leq 5.25 \text{ MeV}) \\ E_e &= 0.63 E_p - 1.10 \text{ MeV} & (E_p > 5.25 \text{ MeV}) \end{aligned} \quad (4.3)$$

the relative behaviour of experimental points is reproduced quite better (fig.15). The reason could be the special electronics using only the fast scintillator pulse part for energy information /21/. That means, the choice of the convenient light response function depends more or less on the electronical integration of the detector pulse for energy information.

For normalization of calculated efficiency curves to experimental points the optimum energy range has to be chosen. It must be high enough to avoid individual properties near threshold, on the other hand the statistical error of experimental points should be small yet. This region seems to be between 3 and 6 MeV. To check this question the  $\chi^2/F$  ratio was calculated for this energy region combining different light response curves due to eq.(4.2) and eq.(4.3), respectively, at the same threshold and also for different thresholds (0.24/0.32 MeV) using the same response function eq.(4.3). In all the cases the  $\chi^2/F$  ratio was smaller than unity showing the usefulness of this method proposed.

Fig.16 shows efficiency curves as result of such procedure. Up to 6 MeV the experimental points have been taken, but for continuation above 6 MeV the normalized Monte Carlo calculations have been used.

References

- /1/ P.Eckstein et al., Nucl.Instr.Meth. 169 (1980) 533
- /2/ S.Mittag et al., report INDC(GDR)-11/L+Special (1980)
- /3/ L.Varnell et al., Nucl.Instr. Meth. 76 (1969) 109
- /4/ W.D.Fromm, report ZfK-243, Rossendorf (1972) 198
- /5/ J.Döring et al., report ZfK-408, Rossendorf (1980) 179
- /6/ S.P.Simakov et al., Proc. of V. Conf. on Neutron Physics, Moscow (1981) 2
- /7/ H.Förtsch & D.Schmidt, TU-Inform. 05-07-82, TU Dresden (1982)
- /8/ S.P.Simakov, FEI Obninsk (1981), private communication
- /9/ M.Drosg, Nucl.Sci.Eng. 67 (1978) 190
- /10/ D.Culley & J.W.Boldeman, report INDC(AUL)-28/G (1978) 29
- /11/ A.B.Smith et al., Nucl.Instr.Meth. 50 (1967) 277
- /12/ A.Smith et al., Nucl.Instr.Meth. 140 (1977) 397
- /13/ M.T.McEllistrem et al., Phys.Rev. C 15 (1977) 927
- /14/ S.P.Simakov et al., Proc. of V. Conf. on Neutron Physics, Kiev (1980) 320
- /15/ D.W.Glasgow et al., Nucl.Sci.Eng. 61 (1976) 521  
C.E.Nelson et al., report BNL-NCS-50681, Brookhaven (1977) 125
- /16/ H.D.Knox et al., Nucl.Sci.Eng. 69 (1979) 223
- /17/ H.Vonach et al., report BNL-NCS-51245, Brookhaven (1980) 343
- /18/ A.Chalupka et al., Nucl.Instr.Meth. 164 (1979) 105
- /19/ M.Adel-Fawzy et al., Kernenergie 24 (1981) 107
- /20/ N.R.Stanton, report OOO-1545-92, Ohio (1971)
- /21/ H.Förtsch et al., TU-Inform. 05-01-80, TU Dresden (1980)

Table 1

Numerical values of the quantities a and b as function of  $\sigma/\lambda$

$y_m$	$\sigma/\lambda$	$\lambda/\sigma$	a	b	$(\sigma/N)f(x_m)$
4	8.447	0.118	2.790	0.76	7.456
3	5.448	0.184	1.205	0.87	4.056
2	3.281	0.305	0.452	1.04	0.356
1	1.859	0.538	0.445	1.29	0.370
0	0.795	1.258	0.795	1.48	0.290
-0.5	0.385	2.597	1.092	1.79	0.207
-1	0.092	10.87	1.506	3.04	0.007
-2	0.007	142.9	2.836	40.2	0.007

Table 2

Unfolding results from two superpositioned lines ( $\Delta K$ : distance per construction,  $x_0$ : distance of unfolded lines; fwhm = 4.6)

$N_1/N_2$	$N_1$	$N_2$	$\sigma$	$\lambda$	$\Delta K$	$x_0$
1:1	10 000	10 000	1.5(fixed)	2.0(fixed)	3	3.00
1:10	1 003	9 997	1.5(fixed)	2.0(fixed)	3	2.99
1:10	1 008	9 991	1.4992	2.0007	3	2.98
1:10	1 775	9 233	1.5(fixed)	2.0(fixed)	1	3.27

Table 3

Separation results of model line from linear background (see fig.5);  $N = 10^4$ ,  $\sigma = 2.0$ ,  $\lambda = 3.0$

backgr. shape	range of sep.	position shift	peak area	$\sigma$	$\lambda$	$\chi^2/F$
straight line	1 to 5	0.00	9999	2.0fixed	3.0fixed	$<10^{-3}$
	3 to 5	0.00	9998	"	"	"
	2 to 5	0.00	9999	2.0022	2.9948	"
constant	3 to 5	-0.06	10717	2.0fixed	3.0fixed	1.0551
	4 to 6	-0.07	10246	"	"	0.4343
	3 to 5	+0.11	11334	2.02026	3.5436	0.0366

Table 4

Averaged asymmetry  $\lambda/\sigma$  for different size of cylindrical samples

sample	height	outer diameter	inner diameter	mass	$\overline{\lambda/\sigma}$
1	4cm	3cm	1cm	45.44g	1.69
2	3cm	2cm	1cm	10.97g	1.71

Table 5

Averaged parameters of neutron lines (sample 2)

	$^{12}\text{C}(n,n_0)$	$^{12}\text{C}(n,n_1)$
measurement 1 $\overline{\text{fwhm}}$ $E_0 = 8 \text{ MeV}$ $\overline{\lambda/\sigma}$	4.64 ns 1.19	6.00 ns 0.74
measurement 2 $\overline{\text{fwhm}}$ $E_0 = 10 \text{ MeV}$ $\overline{\lambda/\sigma}$	4.48 ns 1.55	5.28 ns 1.18
tendencies: $E_0 \downarrow$ fwhm decreases asymm. increases	$n_0 \rightarrow n_1$	fwhm increases asymmetry decreases

Figure Captions

- Fig.1 Neutron lines directly from the target (flight path 3 m) drawn in logarithmic-quadratic coordinates; Gaussian curves would be symmetric to channel  $K = 0$ ; the flight time increases to negative channels.
- Fig.2 Model curves:  $\circ$  corresponding (a),  $x$  - (c) and  $\bullet$  - (d) (the coordinates are logarithmic-quadratic)
- Fig.3 Representations of the function  $f(x;N,x_0,\sigma,\lambda)$  for different ratios  $\sigma/\lambda$
- Fig.4 Comparison of characteristic quantities of the expression  $f(x;N,x_0,\sigma,\lambda)$  calculated according to formula and taken explicitly from real curves; the dash-dotted line is the limit for Gaussian curves
- Fig.5 Model spectrum: peak of type  $f(x;N,x_0,\sigma,\lambda)$  with straight line background; the arrows denote different range limits for fit
- Fig.6 Elastic peak from the  $^{12}\text{C}(n,n)$  reaction and fitted curve in logarithmic coordinates ( $E_0 = 8.0$  MeV,  $\theta_{\text{LAB}} = 40^\circ$ )
- Fig.7 Example for unfolding of a line spectrum
- Fig.8 Example for unfolding of lines with strongly different peak area
- Fig.9 TOF-spectrum of the  $^{93}\text{Nb}(n,n')$  reaction ( $E_0 = 8.0$  MeV,  $\theta_{\text{LAB}} = 80^\circ$ )
- Fig.10 Example for separation of "disturbing" lines with parabolic background:  $\circ$  experimental spectrum,  $\bullet$  fit result,  $+$  background

Fig.11 TOF-spectrum from the  $93\text{-Nb}(n,n')$  reaction ( $E_0 = 12.3$  MeV,  $\theta_{\text{LAB}} = 40^\circ$ ): o experimental points, — fit with model line, ..... free fit procedure, + after subtraction acc. to —, • after subtraction acc. to .....

Fig.12 Angle-integrated energy spectra of the  $93\text{-Nb}(n,n')$  reaction ( $\phi E_0 = 7.0$  MeV,  $\phi E_0 = 7.23$  MeV /8/ ); — integrated from  $40^\circ$  to  $160^\circ$ , ..... integrated from  $20^\circ$  to  $160^\circ$ ; 1 - without elastic peak separation, 2 - separation acc. to method (m2), 3 - separation acc. to method (m1), 4 - separation acc. to method (m3)

Fig.13 Asymmetry measurement of the 252-Cf chamber used

Fig.14 Comparison of Monte Carlo calculations with experimental results ( $\phi$ ) averaged over different detectors and measuring runs; — response function due to eq. (4.2), threshold  $E_e = 0.24$  and  $0.48$  MeV, resp., ..... response function due to eq. (4.3), threshold  $E_e = 0.28$  and  $0.48$  MeV, resp., normalized with factor  $a = 1.387$

Fig.15 Comparison of different Monte Carlo calculations due to eq. (4.2) — and eq. (4.3) ....., respectively

Fig.16 Measured efficiency curves for different detectors combined with calculations (o experimental points with statistical error less 5%, | experimental points with their statistical errors; — Monte Carlo calculation normalized between 4 and 6 MeV by a factor given for each curve; ..... eye-guided line through experimental points)

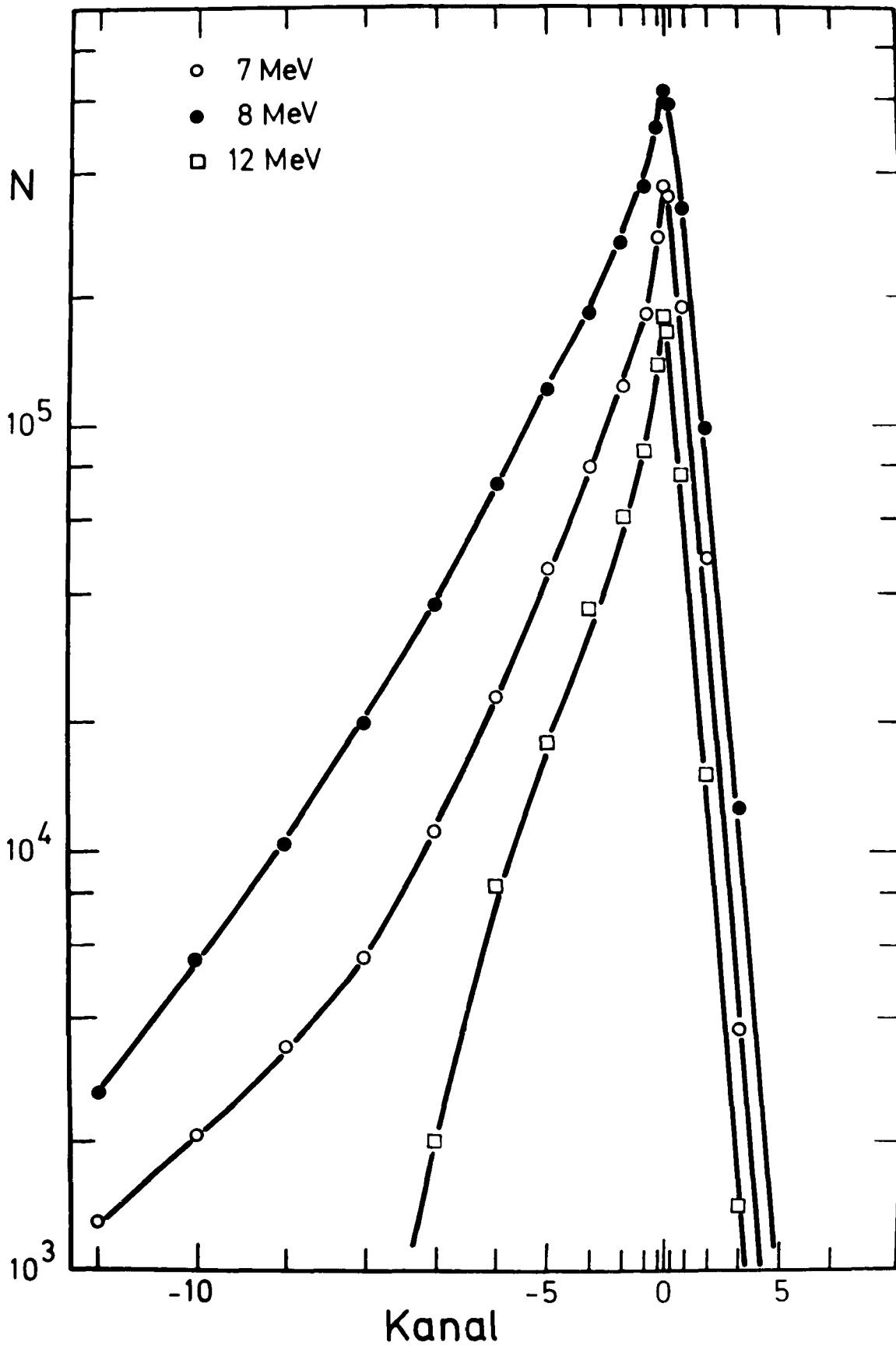


Fig.1

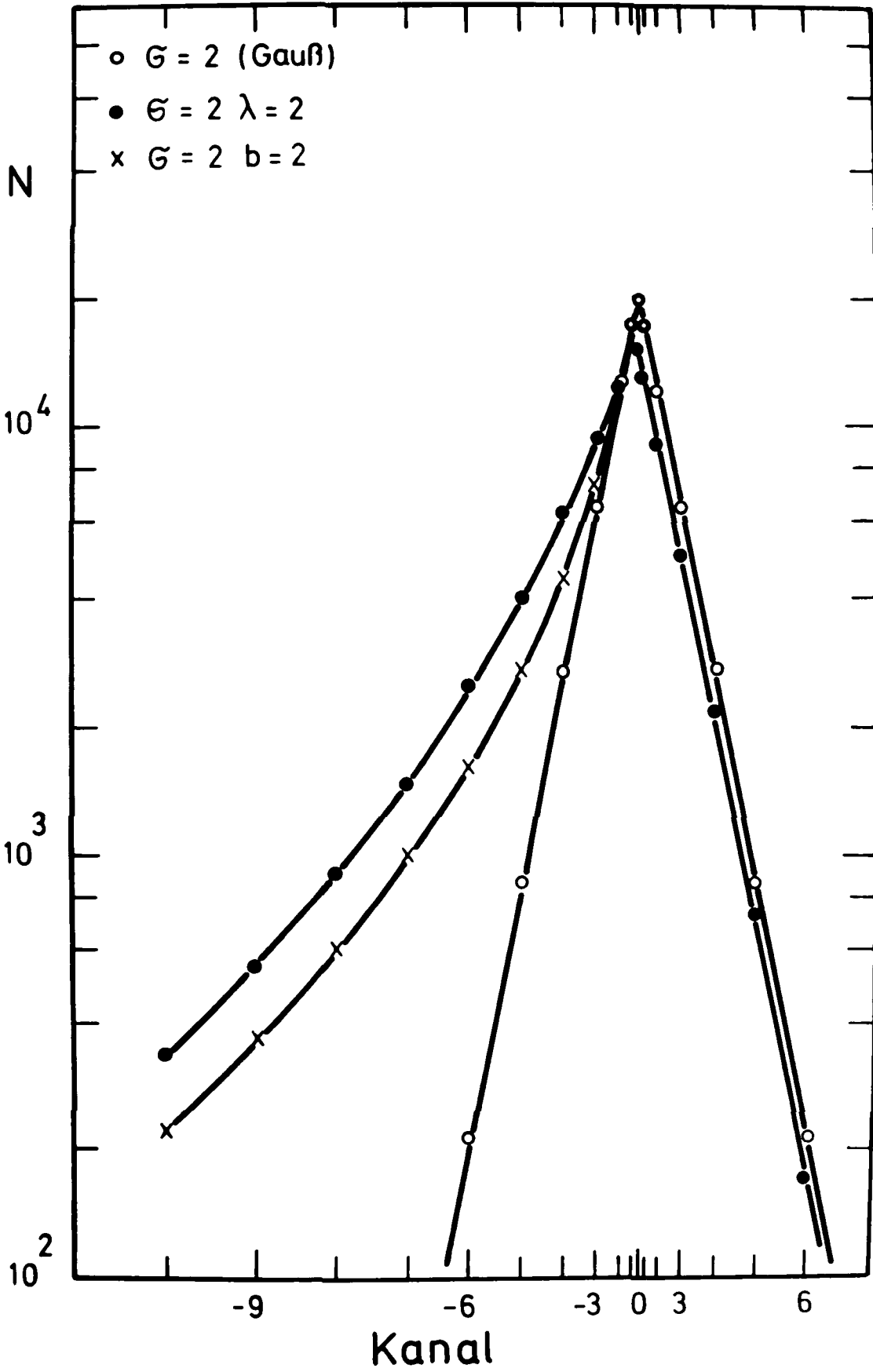


Fig.2

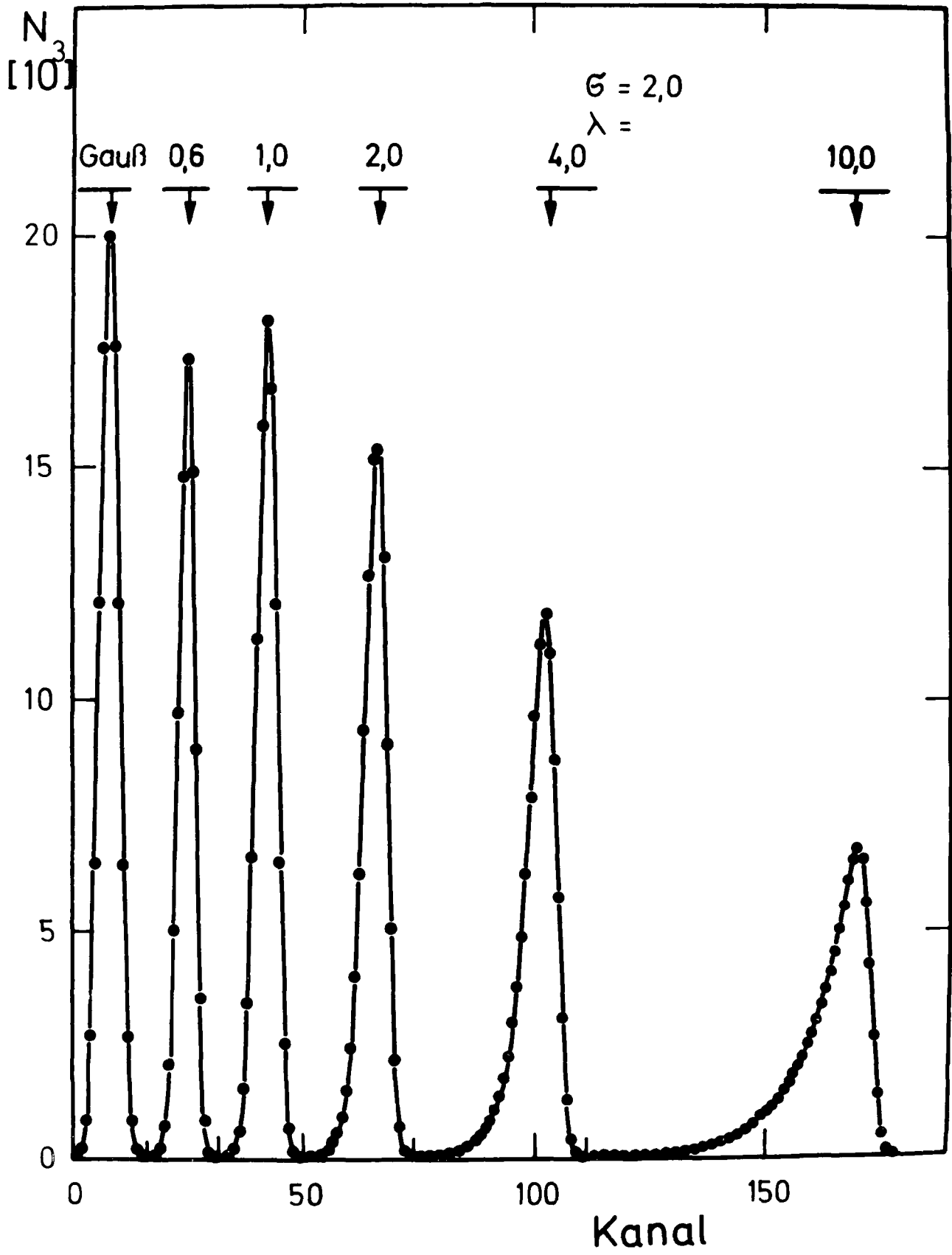


Fig.3

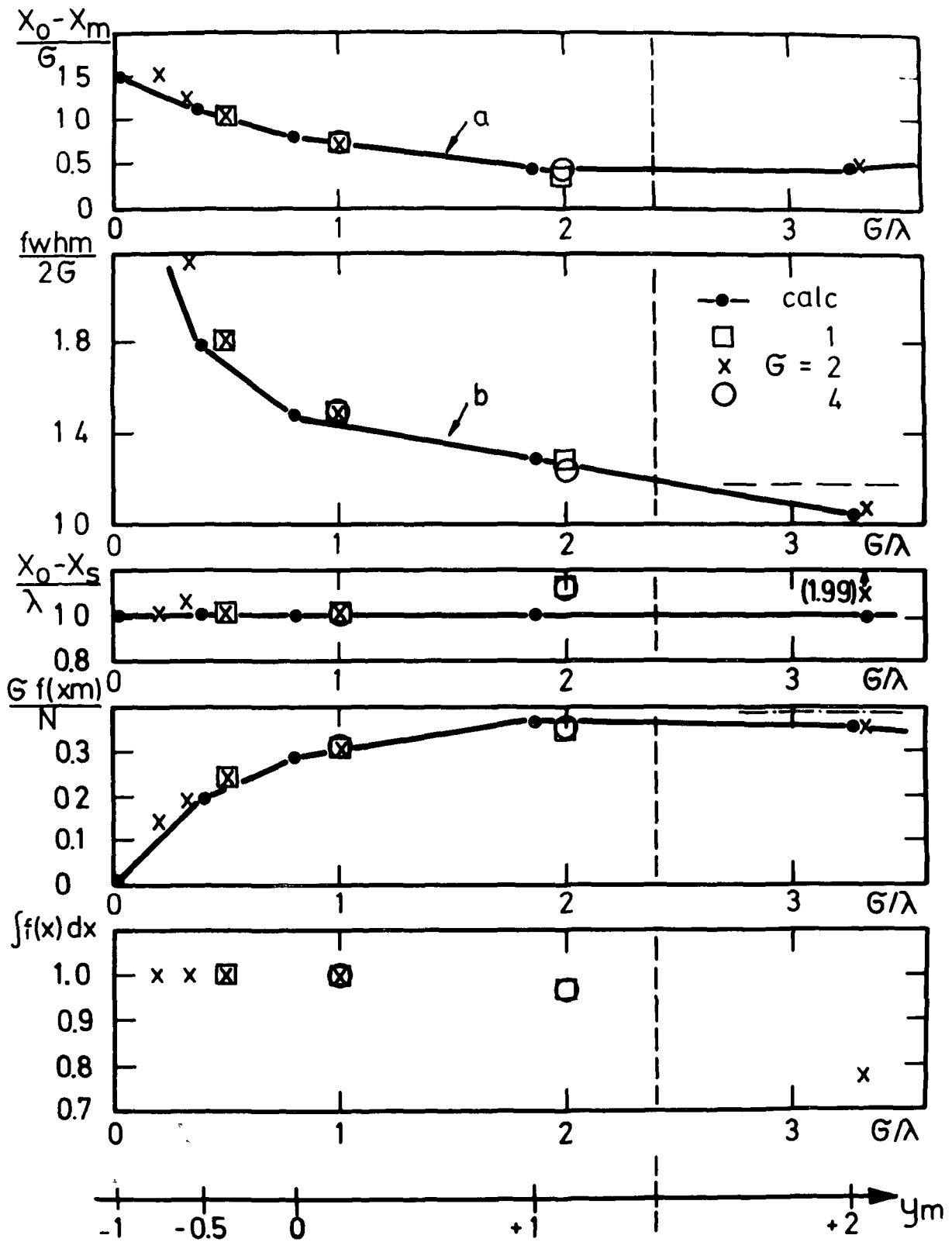


Fig.4

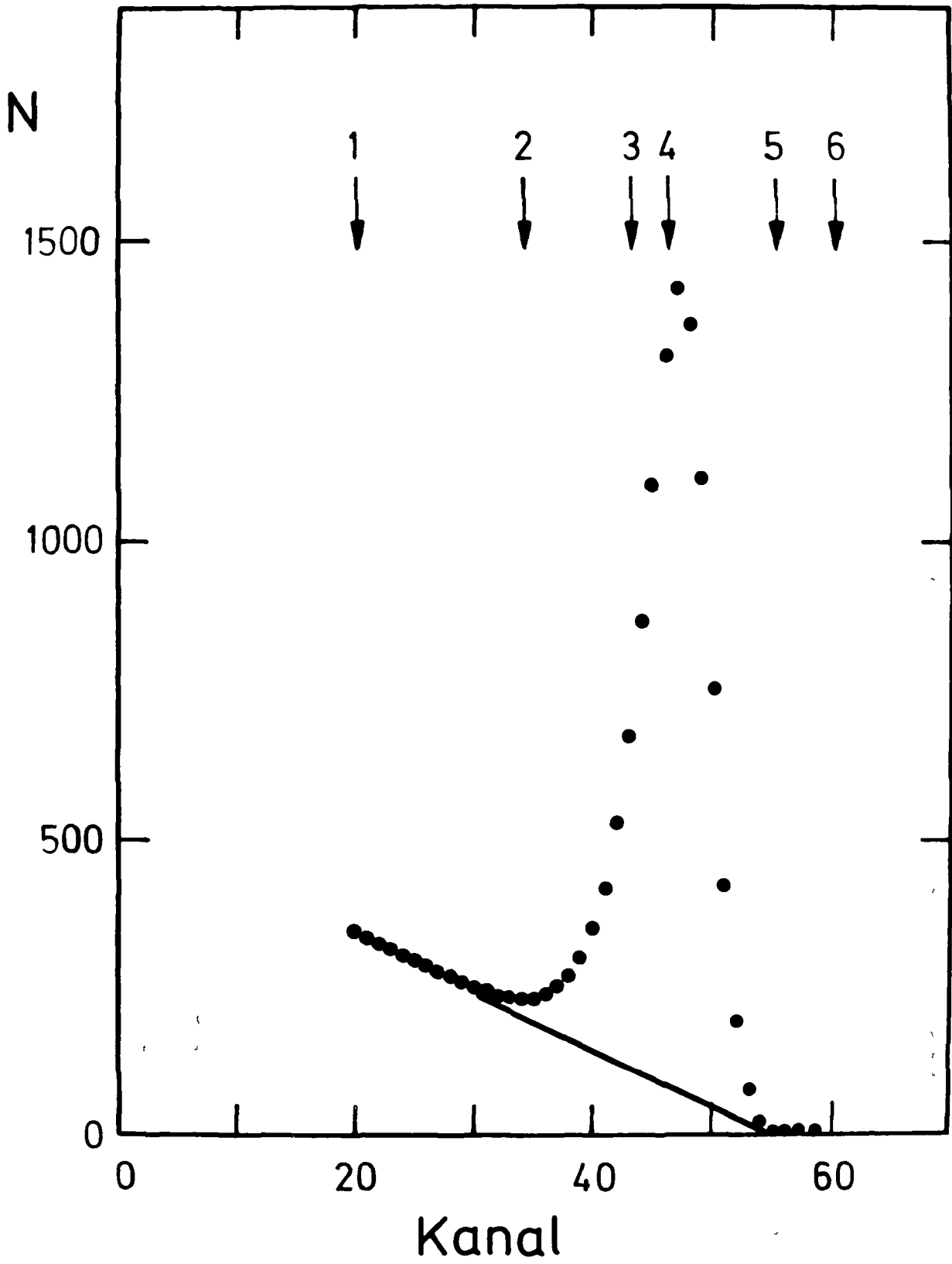


Fig.5

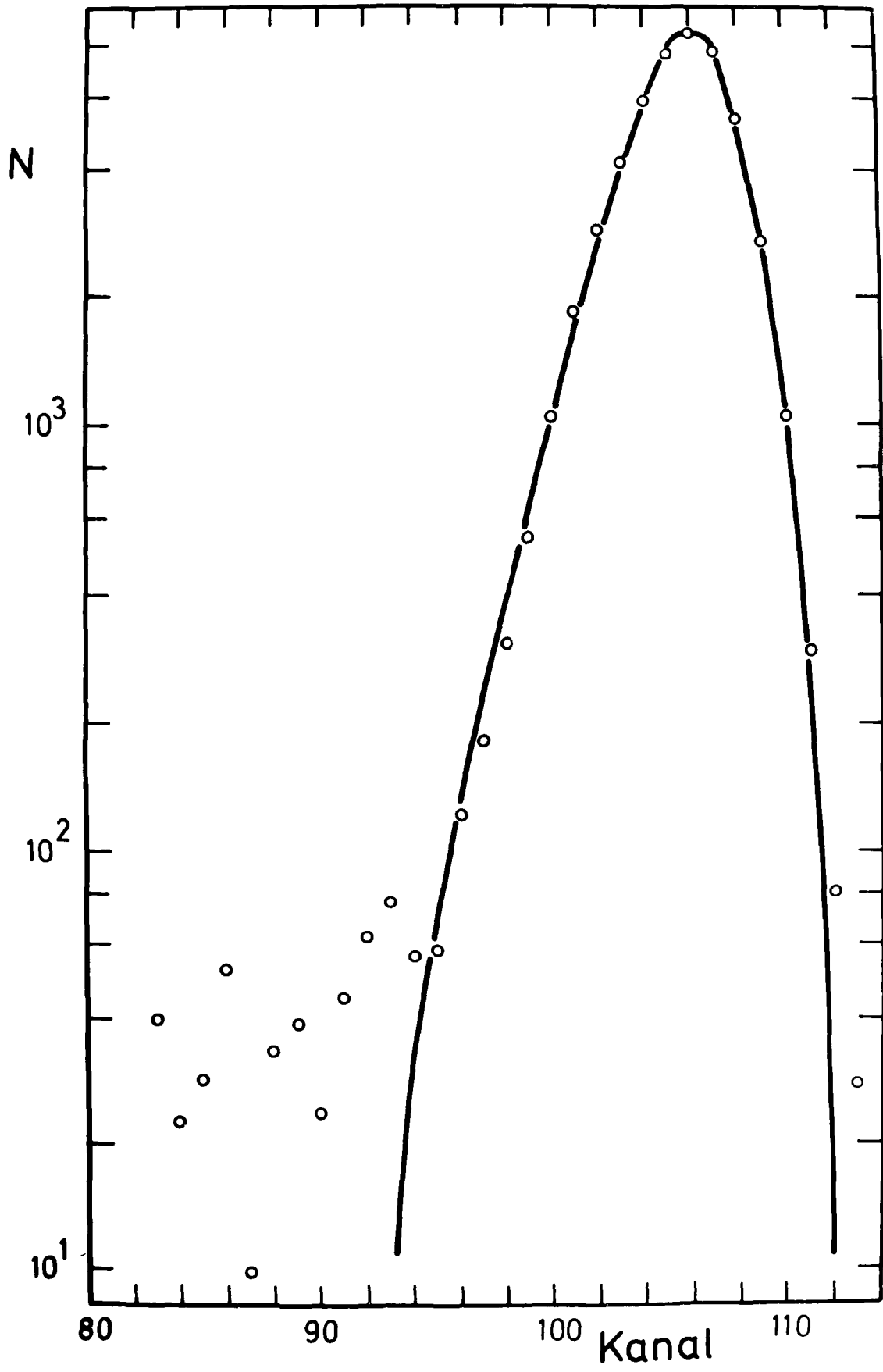


Fig.6

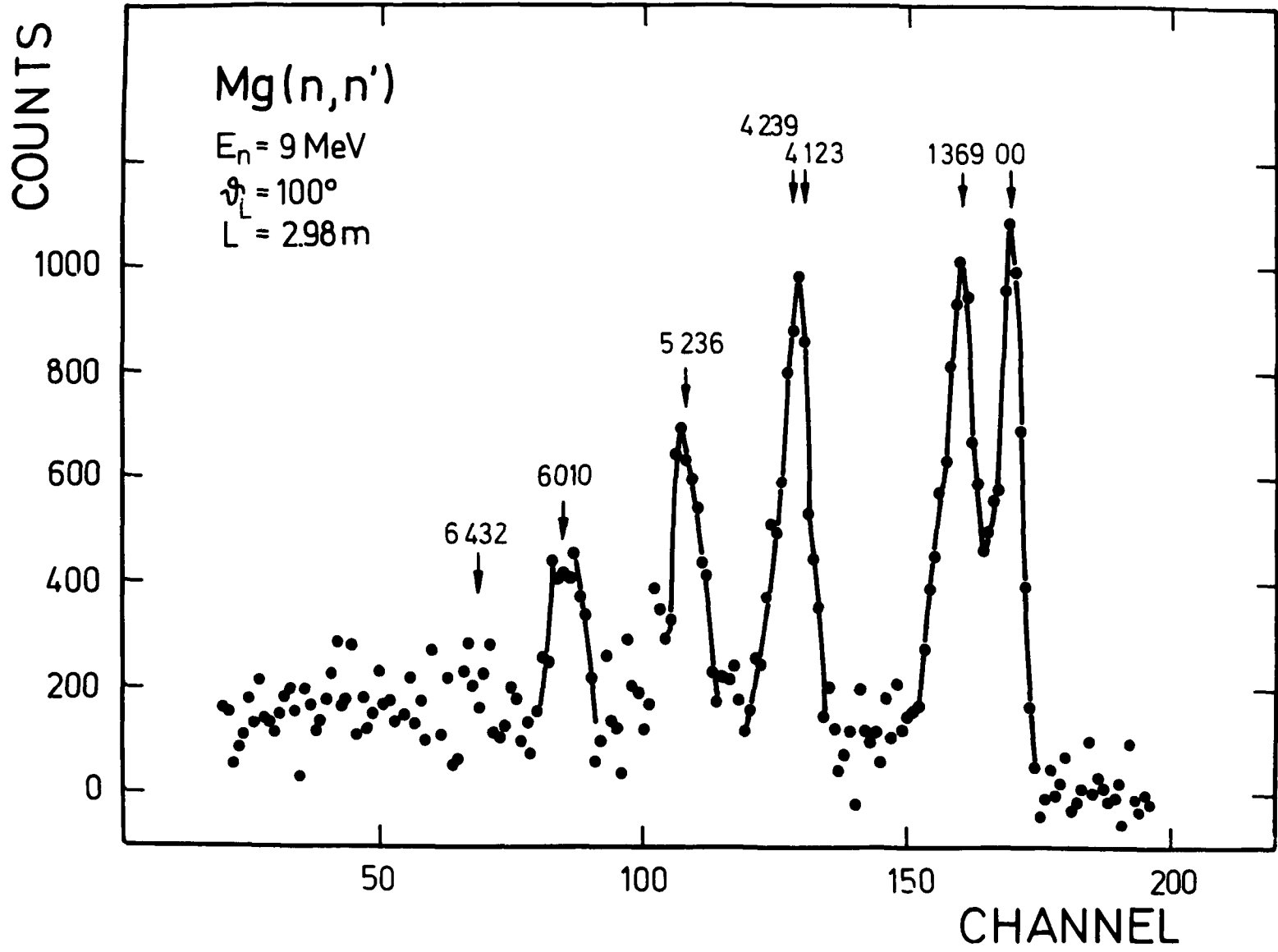


Fig. 7

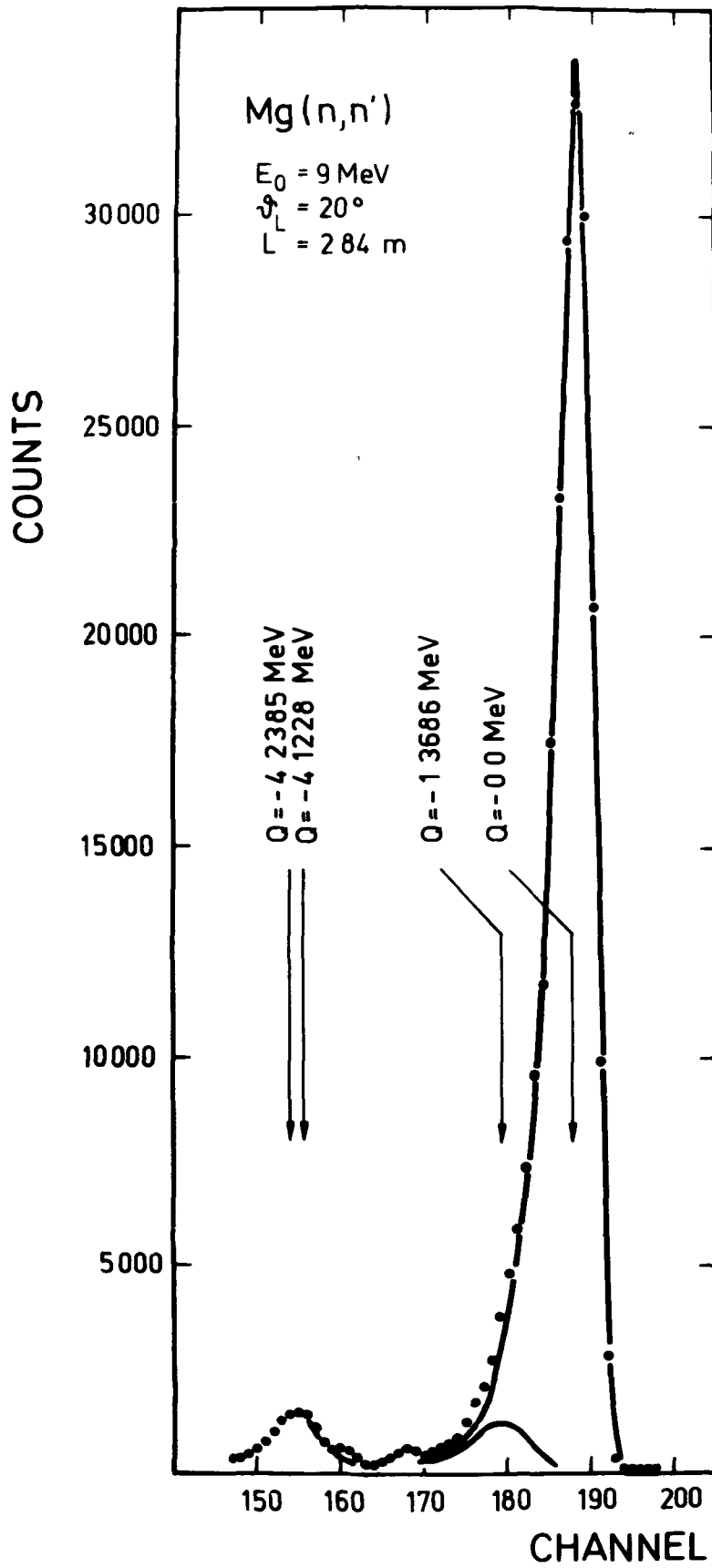


Fig.8

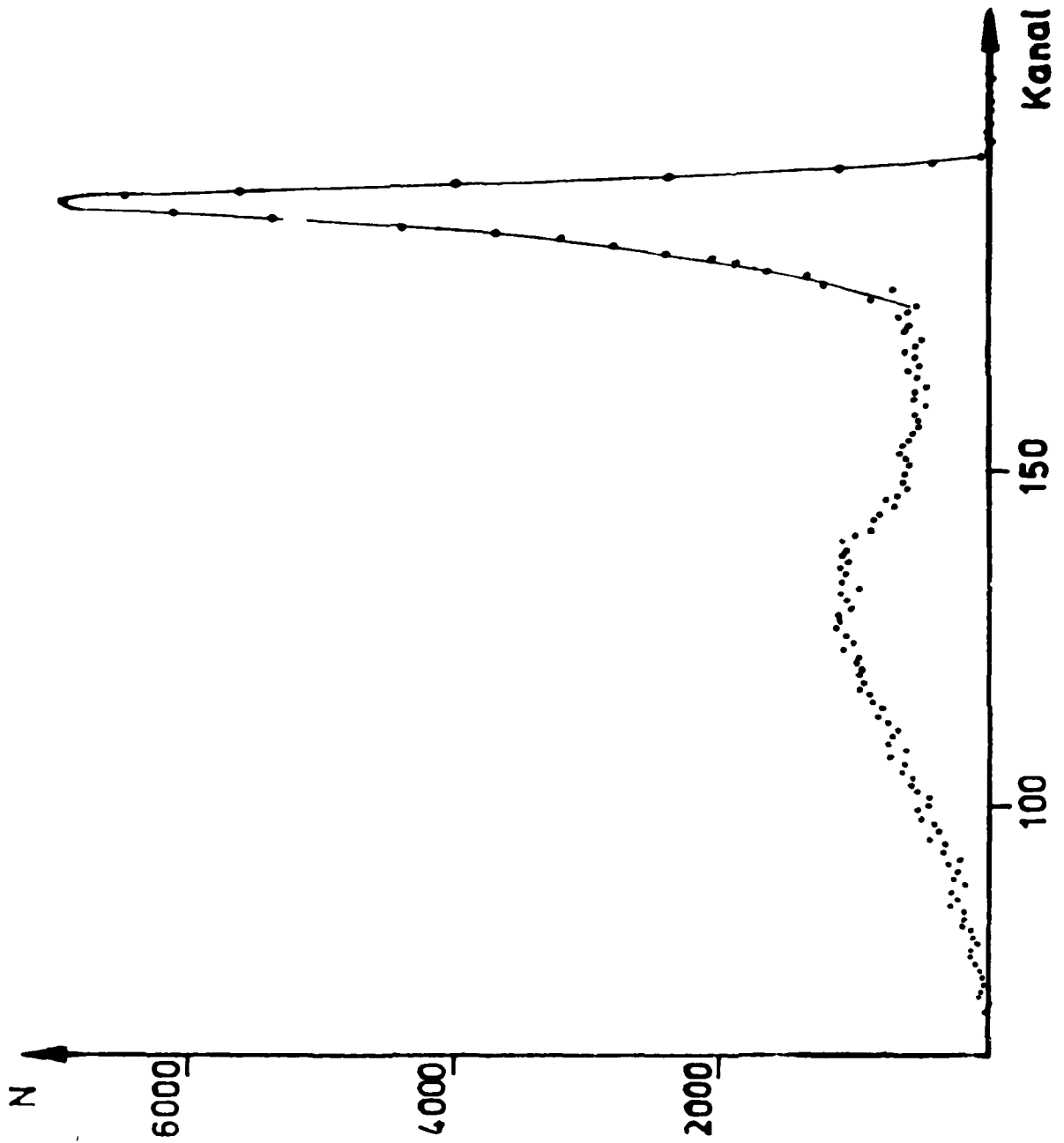
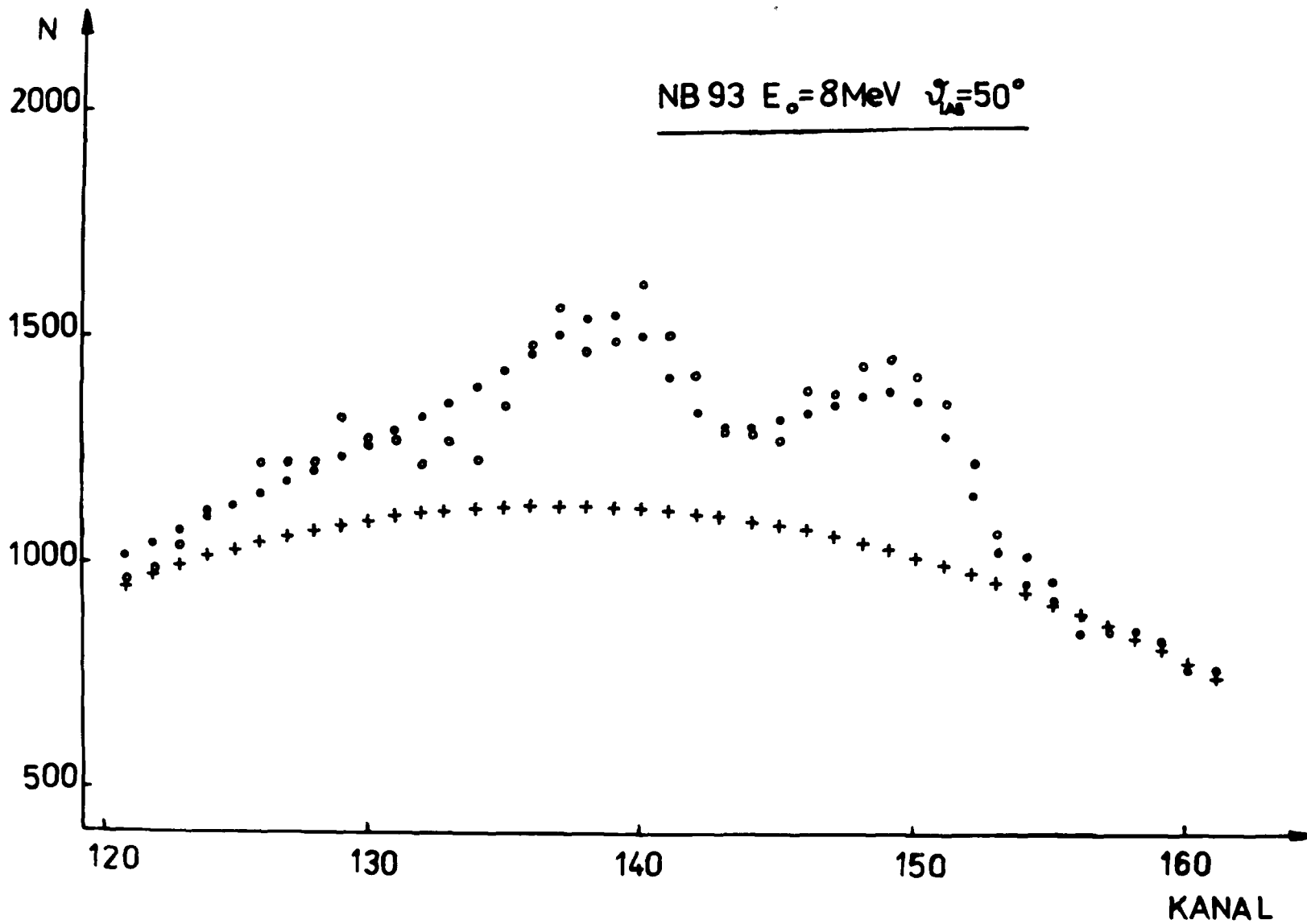


Fig.9

Fig. 10



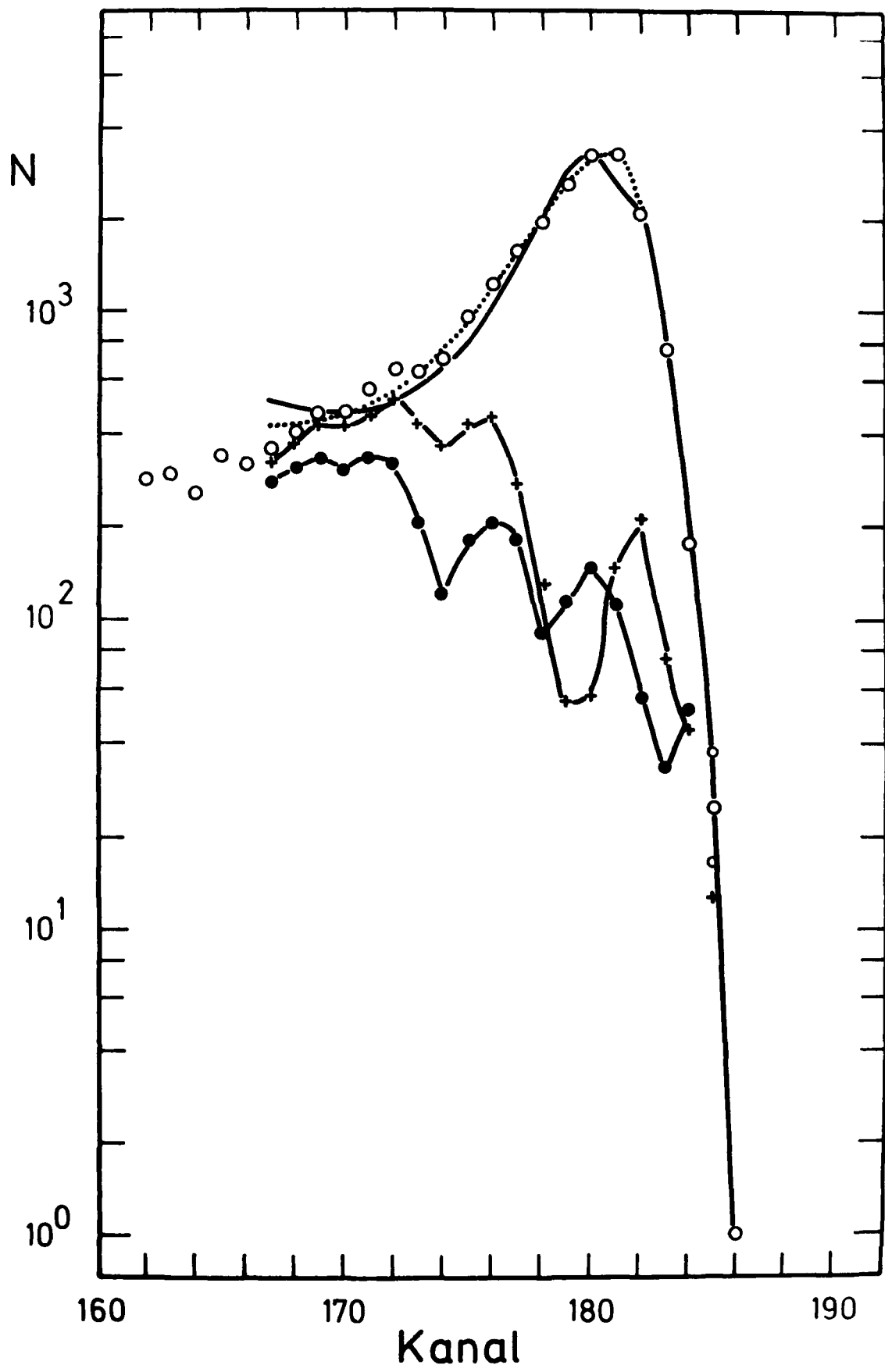


Fig.11

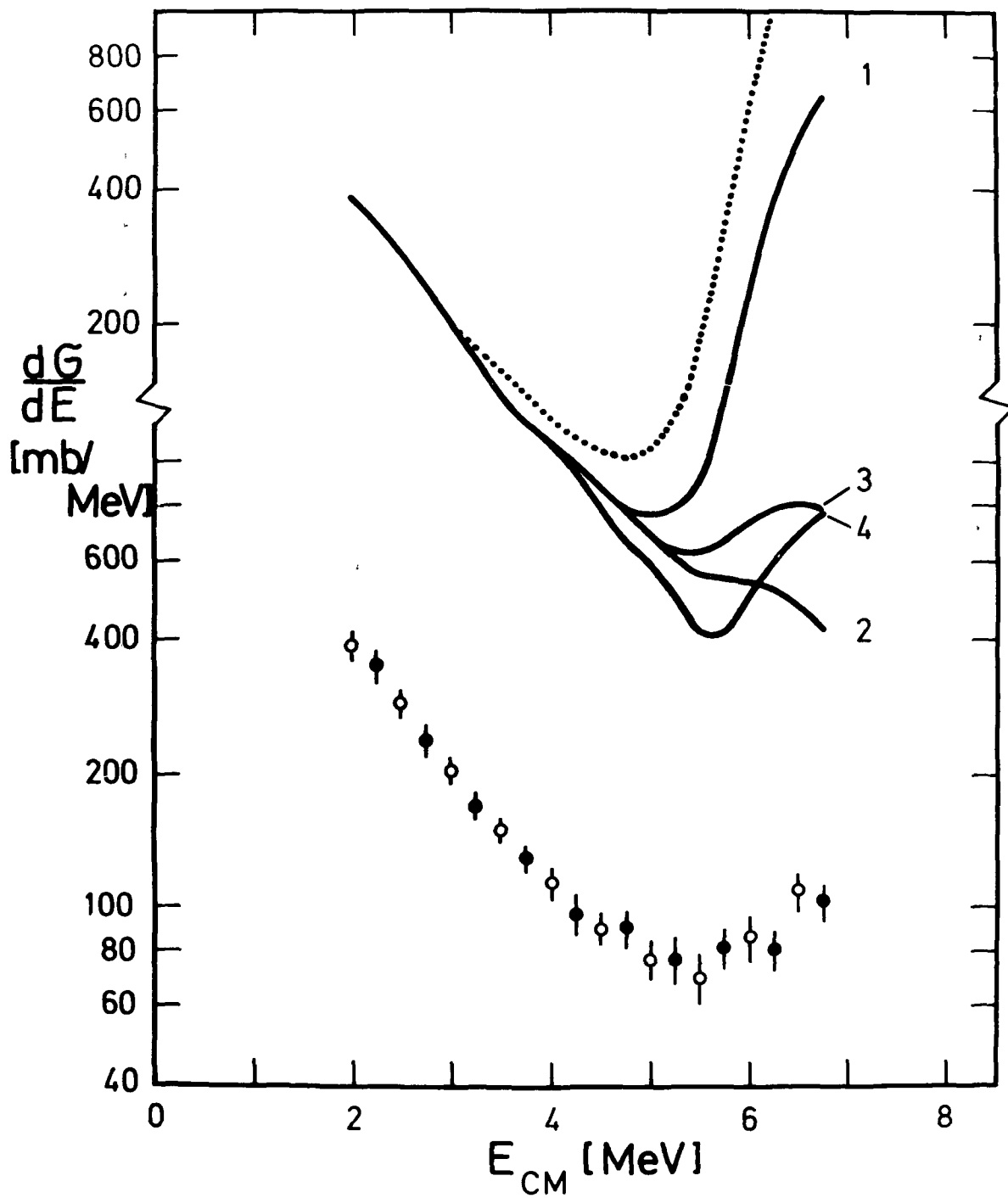


Fig.12

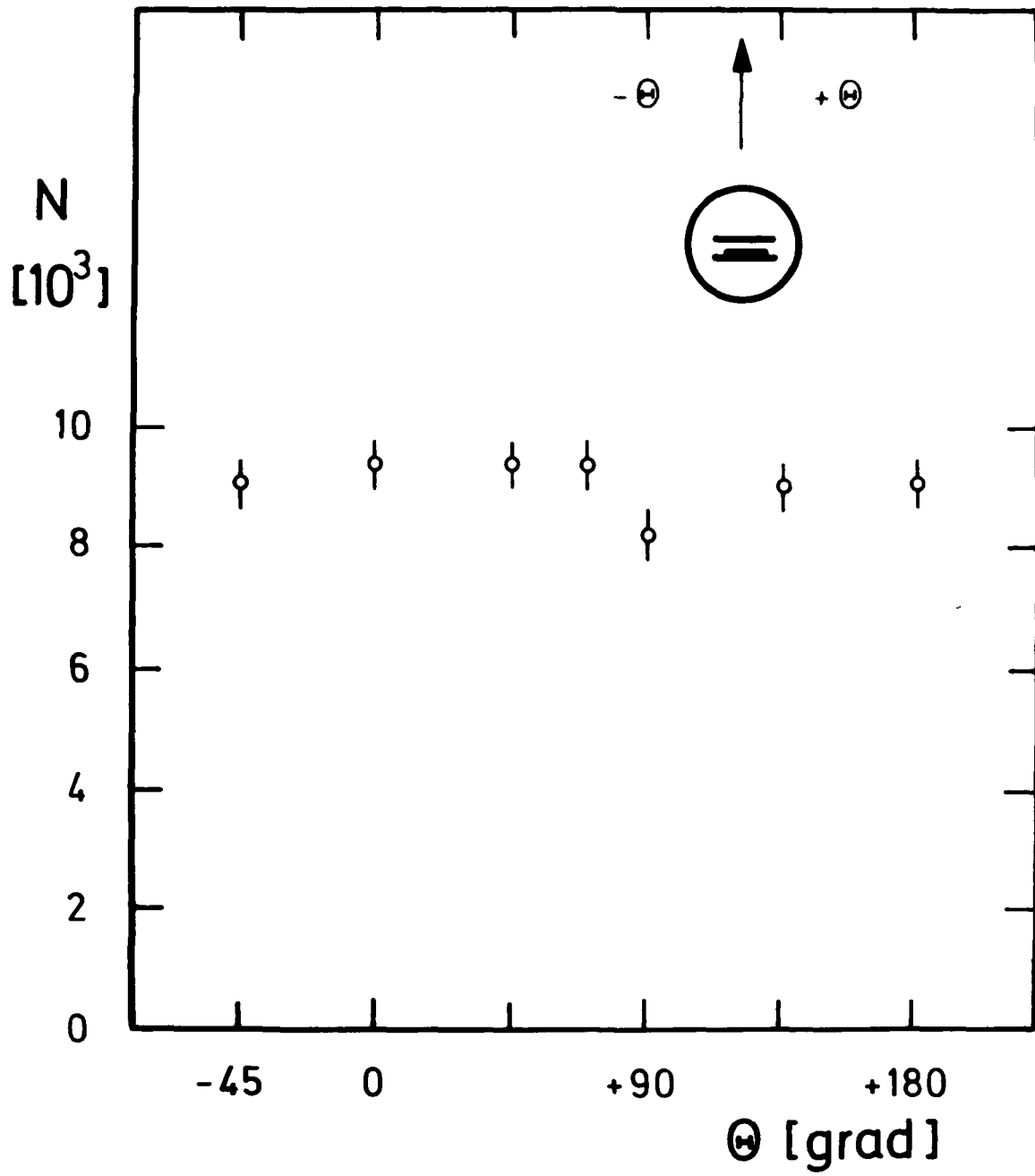


Fig.13

Fig. 14

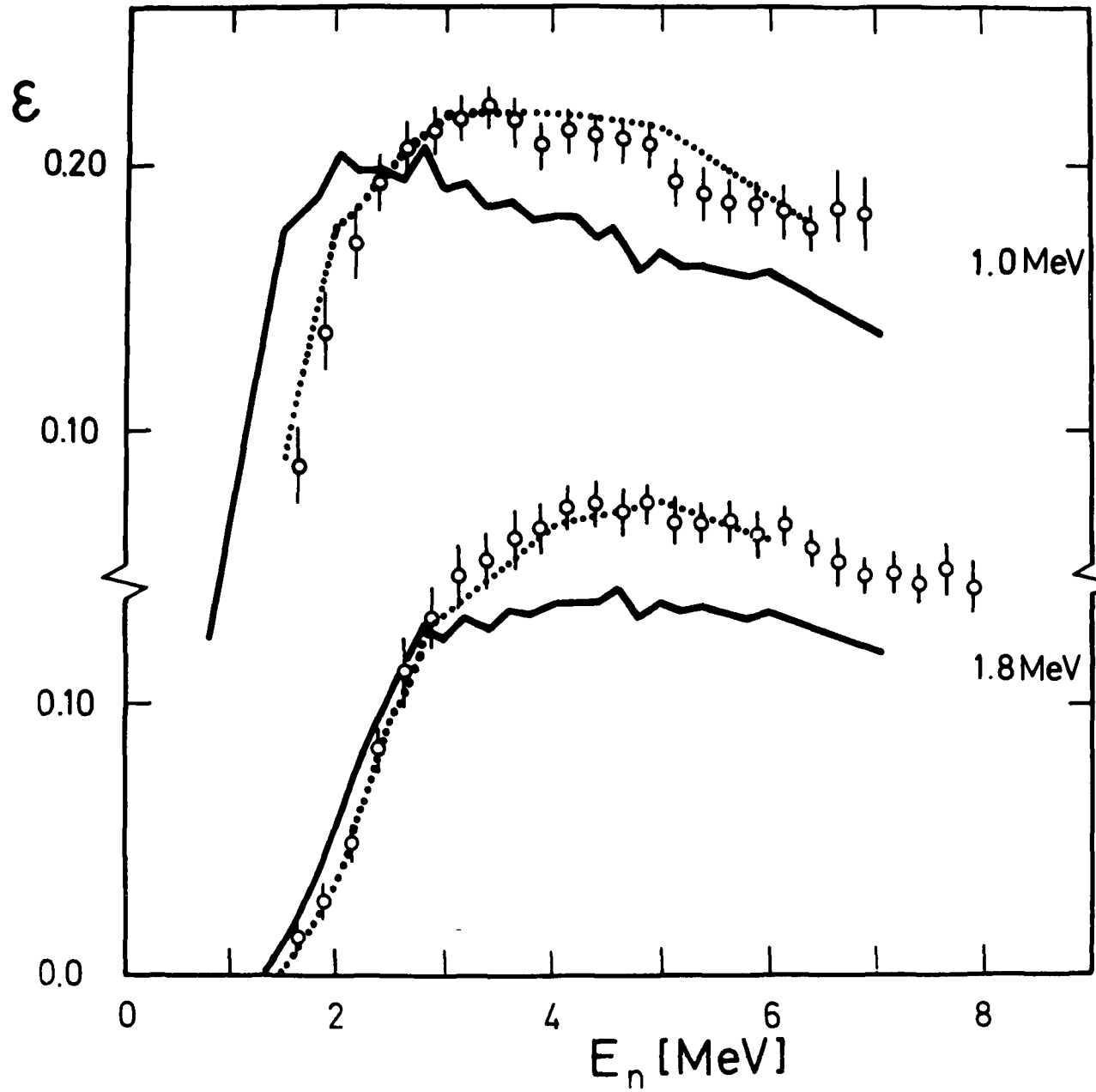
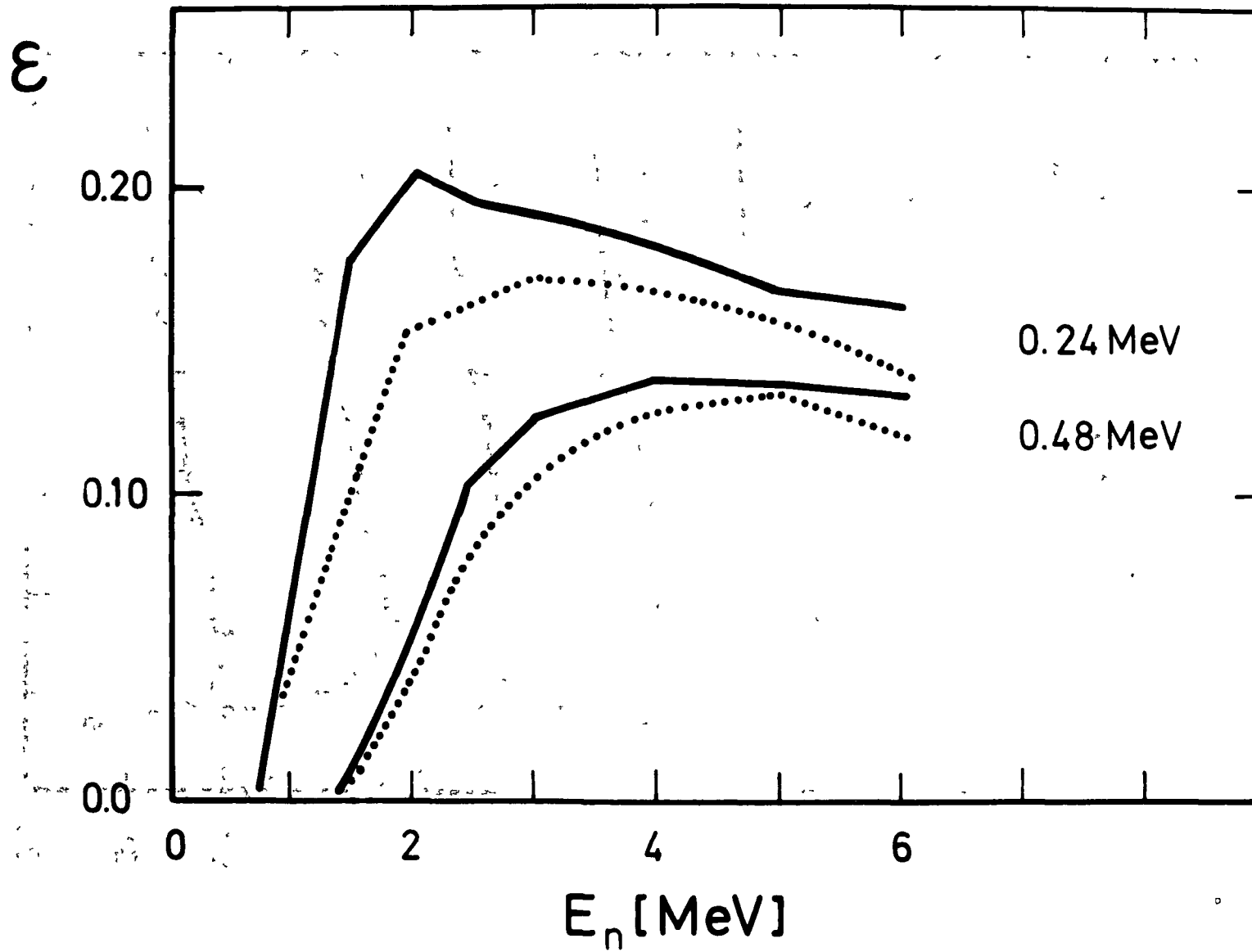


FIG. 15



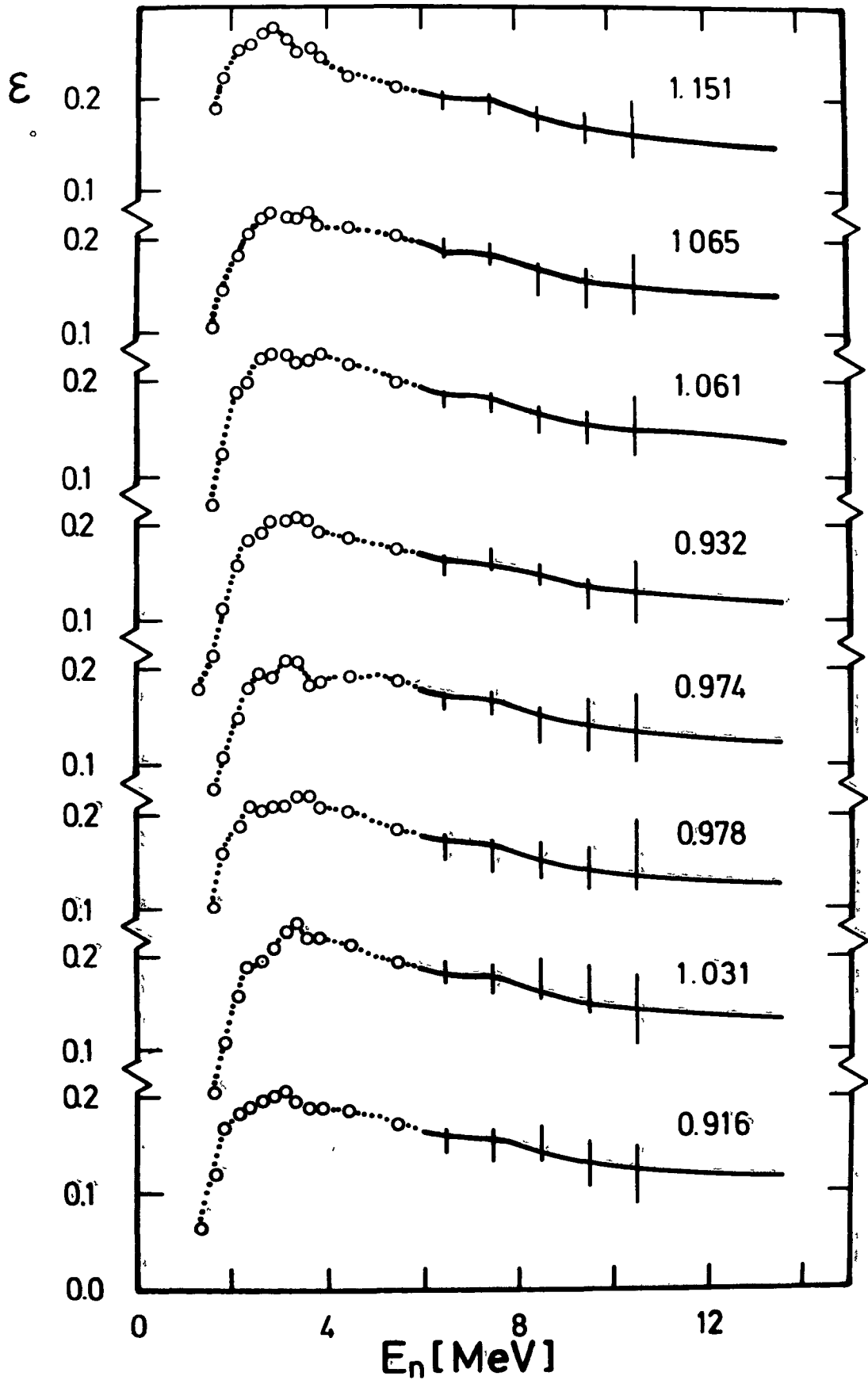


Fig.16